Thermodynamic states and phase diagrams for bulk-incoherent, bulk-coherent, and epitaxially-coherent semiconductor alloys: Application to cubic (Ga,In)N

Jefferson Z. Liu and Alex Zunger
National Renewable Energy Laboratory, Golden, Colorado 80401, USA
(Received 8 January 2008; revised manuscript received 2 April 2008; published 1 May 2008; publisher error corrected 6 May 2008)

The morphology and microstructure of $A_{1-x}B_xC$ semiconductor alloys depend on the type of thermodynamic states established during growth. We distinguish three main cases: (i) *bulk-incoherent* structures occur when the alloy grows without being coherent with an underlying substrate and when each of the possible alloy species—phase separated AC and BC constituents, random $A_{1-x}B_xC$ alloy, or ordered $(AC)_n/(BC)_m$ structures—maintain their own lattice structures and lattice constants, giving up mutual coherence. Bulk incoherence is common in thick films with sufficient dislocations. For cubic (Ga,In)N, bulk-incoherent structures are found to have a positive excess enthalpy $\Delta H_{\mathrm{bulk}}^{\mathrm{incoh}}>0$ and, thus, to phase separate. (ii) *Bulk-coherent* structures occur when the alloy grows without being coherent with a substrate, but each of the possible species internal to the alloy film is forced to be coherent with the film matrix. Thus, the constituents AC-rich and BC-rich solid solution phases share the same lattice structure at their interface, leading to *internal* strain that destabilizes the $AC+BC$ separated constituents. This can expose the intermediate $(AC)_n/(BC)_m$ ordered phases as stable structures with respect to the strained constituents, i.e., $\Delta H_{\mathrm{bulk}}^{\mathrm{coh}}<0$. Bulk coherence is applicable to growth when the development of dislocations is inhibited, e.g., small size precipitates in the alloy matrix. For cubic (Ga,In)N alloy, we find that the coherent ground state phases are three ordered superlattice structures: $(\mathrm{InN})_2/(\mathrm{GaN})_2$ (=chacolpyrite), $(\mathrm{InN})_3/(\mathrm{GaN})_1$, and $(\mathrm{InN})_4/(\mathrm{GaN})_1$, along (201) [and its cubic symmetry equivalent, i.e., (102), (210), etc.] crystal direction. (iii) *Epitaxially coherent* structures occur when the alloy is made coherent with an underlying substrate, e.g., in thin film pseudomorphic growth. Depending on the substrate, the formation enthalpy $\Delta H^{\mathrm{epi}}<0$. For cubic (Ga,In)N grown on GaN (001) substrate, we find that the stablest epitaxial phases are chalcopyrite and the $(\mathrm{InN})_4/(\mathrm{GaN})_1$ superlattice along the (210) crystal direction. Here, we calculate, from first principles, the formation enthalpies of cubic zinc blende (Ga,In)N alloy under the three forms of thermodynamic states indicated above to establish a cluster expansion, from which we calculate the finite-temperature phase diagrams. This illustrates how the thermodynamic constraints during growth can radically alter the alloy phase behavior and its microstructures.

DOI: 10.1103/PhysRevB.77.205201 PACS number(s): 64.70.kg, 61.66.Dk, 64.75.Qr, 64.75.St

I. INTRODUCTION

For many semiconductor applications, it is desired to have material properties that are intermediate between those offered by pure binary semiconductor compounds. A traditional way to achieve this is to create solid solutions of two or more such "building blocks," i.e., by alloying.[1,2] These alloys or solid solutions are often viewed as random substitution of alloyed elements on sites of the parent lattice. In reality, however, perfect randomness only rarely occurs, and various deviations from it, such as long-range ordering, short-range ordering, clustering, and phase separation (see Refs. 1 and 2 and references therein), were experimentally noted. Such microstructures decide much of the electronic, optical, and transport properties of the alloy system. For example, the optical band gap and transport effective mass of ordered alloys are significantly different from those of random alloys at the same chemical composition,[1] and the carrier mobility in phase-separated alloys can be very different from that in ordered structures.[3]

In addition to kinetic effects,[4] it is now understood that such microstructures of $A_{1-x}B_xC$ semiconductor alloys are decided to a large extent by the constrained thermodynamics of the system during its growth.[1,5–9] Such constraints include the coherent strain from the generally lattice mismatched AC vs BC alloy components, strain from the underlying substrate, and reconstruction-induced strain from the exposed surface in gas-phase-epitaxy [e.g., metal-organic chemical vapor deposition (MOCVD) and molecular beam epitaxy (MBE)] growth. Such constraints can have dramatic influences on the alloy's thermodynamic stability. An example is the *substrate-coherent epitaxy-induced film thermodynamics*.[5,6,10] In this case, the equilibrium solid solubility is enhanced because phase-separation into substrate-coherent constituents (AC on substrate) and (BC on substrate) has a higher energy and, thus, is suppressed by the elastic energy cost to lattice matching. Another example is the *surface-reconstruction-induced subsurface long-range ordering*.[1] In this case, surface reconstruction creates strain patterning in a few subsurface layers[8,9] and leads, in turn, to an energetic driving force for selective incorporation of the smaller (larger) of two alloy atoms at high (low) strain subsurface sites, leading to the formation of long-range ordered $(AC)_1/(BC)_1$ CuPt-like phases.[11] The role of such external constraints on semiconductor alloy thermodynamics and ensuing microstructures were extensively studied in the past and reviewed in Refs. 1 and 2.

In this paper, we discuss three thermodynamic states of semiconductor alloys that do not involve the effects of a free surface during growth ("surface reconstruction-induced surface ordering"). These are *bulk-incoherent thermodynamics*, *bulk-coherent thermodynamics*,[12] and *substrate-coherent ep-*

 ©2008 The American Physical Society

itaxial thermodynamics.[1] The purpose of this paper is to describe the constraints characterizing these cases, to provide a first-principles calculation of the relevant energetics, and to provide the corresponding phase diagrams. These ideas will be illustrated for cubic zinc blende (Ga,In)N alloy.

II. CONSTRAINED AND UNCONSTRAINED EXCESS ENERGIES

We define two characteristic energies for pseudobinary $A_{1-x}B_xC$ alloy systems: the excess energy ΔE of the unconstrained alloys and the excess energy δE of the constrained alloys:

(a) *Excess energy of the unconstrained system* $\Delta E(\sigma)$: This is the total-energy difference between a configuration σ (a particular assignment of A and B atoms to lattice sites) at its equilibrium lattice constant a_σ, with respect to equivalent amounts of the pure AC and BC solid constituents at their own (unconstrained) equilibrium lattice constants a_{AC} and a_{BC}, respectively,

$$\Delta E(\sigma) = E(x,\sigma) - [(1-x)E_{AC}(a_{AC}) + xE_{BC}(a_{BC})]. \quad (1)$$

The excess energy in Eq. (1) (also called formation energy) is the energy gain or loss when mixing pure AC and BC to form the alloy configuration σ and thus represents the natural cohesive tendency of structure σ.

(b) *Excess energy of the constrained system* $\delta E^{(c)}(\sigma)$: When the compound or alloy σ is constrained in some way (e.g., strain from a substrate etc.), its energy changes from $E(\sigma)$ to $E^{(c)}(\sigma)$. The excess energy of the constrained system is thus

$$\delta E^{(c)}(\sigma) = E^{(c)}(x,\sigma) - E^{(c)}(AC+BC). \quad (2)$$

These two characteristic energies $\Delta E(\sigma)$ and $\delta E^{(c)}(\sigma)$ can be used to describe the energetic properties (i.e., formation enthalpy ΔH) of the three thermodynamic states of semiconductor alloys: bulk-incoherent thermodynamics, bulk-coherent thermodynamics, and substrate-coherent epitaxial thermodynamics.

III. THREE ALLOY THERMODYNAMIC STATES IN THE ABSENCE OF FREE SURFACES

In this section, we describe the qualitative physics distinguishing the three alloy thermodynamic states in the absence of a free surface. Section IV will provide computational details.

A. Bulk-incoherent structures

A bulk-incoherent alloy is a system in which each of the possible alloy species—phase separated AC and BC constituents, random $A_{1-x}B_xC$ alloy or ordered $(AC)_n/(BC)_m$ structures—maintain their own lattice structures and lattice constants, giving up mutual coherence. There is no substrate and no free surface, but the sample may have defects, such as dislocations and grain boundaries, to accommodate the different phases in real samples. Since these different phases AC, BC, and $A_{1-x}B_xC$ are no longer necessarily located on a single parent lattice with the same lattice constant, we call this type of system "bulk incoherent," wherein the lack of coherence is internal to the alloy (not with respect to an external substrate). This term refers to the traditional description of alloy in classical metallurgy.[13] For this traditional system, the formation enthalpy $\Delta H^{\text{incoh}}_{\text{bulk}}$ is the excess energy of the unconstrained system $\Delta E(\sigma)$ [Eq. (1)],[14]

$$\Delta H^{\text{incoh}}_{\text{bulk}}(\sigma) = \Delta E(\sigma). \quad (3)$$

A large lattice mismatch between components of a III-V zinc blende semiconductor $A_{1-x}B_xC$ alloy normally leads to the positive formation enthalpy Eq. (3).[1,15–17] Therefore, its thermodynamics is characterized by a miscibility gap in the composition (x)-temperature (T) phase diagram, below which the alloy will phase separate into AC-rich and BC-rich solid solution phases at their own incoherent equilibrium lattice constants a_{AC} and a_{BC}.[16] The incoherence between the parent alloy phase $(AC)_{1-x}(BC)_x$ and its phase-separated constituents $(1-x)AC+xBC$ is accommodated in real samples by a high density of defects, such as dislocations, or grain boundaries at the interface of these phases.

B. Bulk-coherent structures

When a three-dimensional bulk alloy system maintains its lattice coherence between an $A_{1-x}B_xC$ alloy and an $AC+BC$ phase separation or an ordered $(AC)_m/(BC)_n$ structure, we call this system bulk coherent. There is no substrate nor free surface in this case. The constrained energy $E^{(c)}(x,\sigma)$ in Eq. (2) equals the total energy $E(x,\sigma)$ in Eq. (1), but in contrast to the bulk-incoherent case, the constituents AC-rich and BC-rich solid solution phases share the same lattice constant $a_\perp$ at their interface, leading to a strain energy because of the lattice mismatch between AC and BC. Consequently, the energy $E^{(c)}(AC+BC)$ [Eq. (2)] equals $(1-x)E_{AC}(a_{AC}) + xE_{BC}(a_{BC}) + U^{\text{coh}}(x)$, where $U^{\text{coh}}(x)$ is the strain energy cost to maintain lattice coherence at the interface. Thus, the formation enthalpy in such bulk-coherent alloy $\Delta H^{\text{coh}}_{\text{bulk}}(\sigma)$ [Eq. (2)] is

$$\Delta H^{\text{coh}}_{\text{bulk}}(\sigma) = \delta E^{(c)}(\sigma) = E(x,\sigma) - [(1-x)E_{AC}(a_{AC}) + xE_{BC}(a_{BC})] - U^{\text{coh}}(x). \quad (4)$$

The coherent strain energy $U^{\text{coh}}(x)$ can be described by the constituent strain energy $\Delta E_{CS}(\hat{\boldsymbol{k}},x)$ (Ref. 18) along the interface direction $\hat{\boldsymbol{k}}$ and at a composition x. It is defined as the elastic energy cost to form lattice matching at the interface of two semi-infinite slab AC and BC of orientation $\hat{\boldsymbol{k}}$,

$$\Delta E_{CS}(\hat{\boldsymbol{k}},x) = \min_{a_\perp}[(1-x)\Delta E^{\text{epi}}_{AC}(\hat{\boldsymbol{k}},a_\perp) + x\Delta E^{\text{epi}}_{BC}(\hat{\boldsymbol{k}},a_\perp)], \quad (5)$$

where $\Delta E^{\text{epi}}_{AC}(\hat{\boldsymbol{k}},a_\perp)$ is the strain energy required to biaxially deform AC to lattice constants $a_\perp$ at an interface $\hat{\boldsymbol{k}}$ from its equilibrium lattice constants a_{AC}. Both $\Delta E^{\text{epi}}_{AC}(\hat{\boldsymbol{k}},a_\perp)$ and $\Delta E^{\text{epi}}_{BC}(\hat{\boldsymbol{k}},a_\perp)$ are positive definite. For a fixed concentration, the minimum constituent strain energy $\Delta E^{\min}_{CS}(x) = \min_{\hat{k}}[\Delta E_{CS}(\hat{\boldsymbol{k}},x)]$ with respect to the interface direction $\hat{\boldsymbol{k}}$

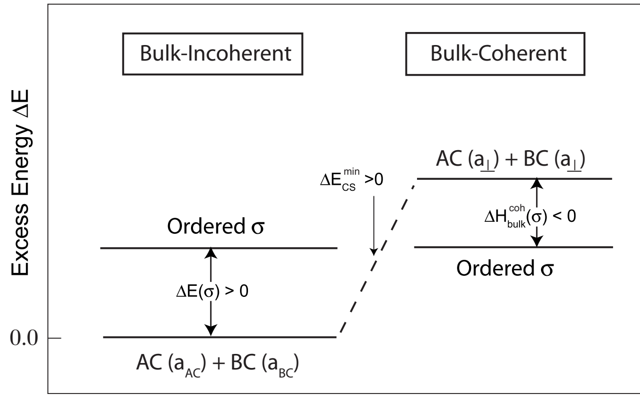

FIG. 1. Schematic plot of energetic orders in bulk-incoherent and bulk-coherent alloys. Because of the lattice mismatch between AC and BC, the ordered structure σ has a higher energy than that of incoherent phase separation $AC(a_{AC})+BC(a_{BC})$, i.e., $\Delta E(\sigma)>0$. In the bulk-coherent state, the strain energy cost $\Delta E_{CS}^{\min}(x)$ to maintain the lattice coherence for AC-rich and BC-rich solid solutions at the interface increases the coherent phase separation energy and, thus, the formation enthalpy $\Delta H_{\text{bulk}}^{\text{coh}}(\sigma)$ in the bulk-coherent state becomes negative.

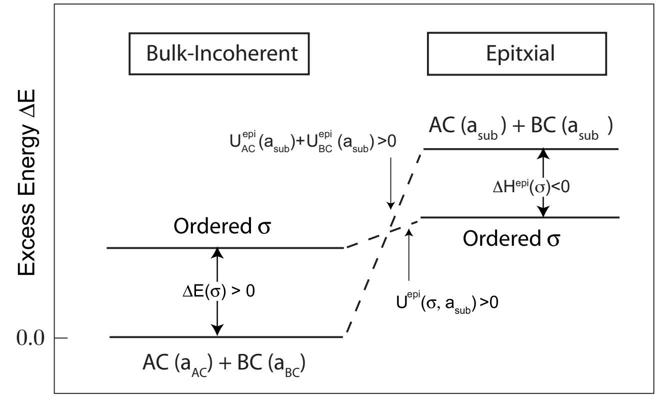

FIG. 2. Schematic plot of energetic orders in bulk-incoherent and substrate-coherent epitaxial alloys. Because of the lattice mismatch between AC and BC, the ordered structure σ has a higher energy than that of incoherent phase separation $AC(a_{AC})+BC(a_{BC})$, i.e., $\Delta E(\sigma)>0$. In the presence of the substrate, the strain energy $U^{\text{epi}}(\sigma,a_{\text{sub}})$ destabilizes the phase separation $AC(a_{\text{sub}})+BC(a_{\text{sub}})$ and then the formation enthalpy $\Delta H^{\text{epi}}(\sigma)$ becomes negative.

characterizes the strain energy $U^{\text{coh}}(x)$. The formation enthalpy $\Delta H_{\text{bulk}}^{\text{coh}}(\sigma)$ [Eq. (4)] can then be expressed as

$$\Delta H_{\text{bulk}}^{\text{coh}}(\sigma) = \Delta E(\sigma) - \Delta E_{CS}^{\min}(x). \tag{6}$$

As we will see below (Sec. IV B), coherent strain energy is minimal at $\hat{\boldsymbol{k}}=(100)$.

The coherent strain energy $\Delta E_{CS}^{\min}(x)$ for a bulk zinc blende semiconductor alloy is positive definite. In comparison to Eq. (3), the formation enthalpy $\Delta H_{\text{bulk}}^{\text{coh}}(\sigma)$ of bulk-coherent alloy will be reduced from bulk-incoherent formation enthalpy $\Delta H_{\text{bulk}}^{\text{incoh}}(\sigma)$ and could even become negative. Figure 1 schematically shows the effect of lattice coherent strain on the energetic order of various phases in such a system. We see that bulk coherence can destabilize the constituents by increasing their energy by $\Delta E_{CS}^{\min}(x)$, thereby converting the positive formation enthalpy $\Delta H_{\text{bulk}}^{\text{incoh}}(\sigma)>0$ to negative values $\Delta H_{\text{bulk}}^{\text{coh}}(\sigma)<0$ for some ordered structure σ under coherent conditions. This could lead to ordering even without substrate or surface reconstruction.[16,17]

C. Substrate-coherent epitaxial structures

Here, we consider the case wherein the film grows on a substrate but free surfaces are not present. Due to the potential lattice mismatch between the $A_{1-x}B_xC$ alloy film and the underlying substrate in epitaxial growth, the alloy film experiences elastic strain applied from the substrate. If the thickness h of the film is above a critical value h_c,[19] the film starts to develop misfit dislocations, lowering its energy toward the fully relaxed bulk value. In this section, our discussion is limited to the situation wherein the film keeps strict coherent registry with the substrate ($h \leq h_c$). The effect of epitaxial strain on the thermodynamic properties of thin film alloy has already been extensively studied in the past.[1,2,6,7,10] The purpose of this section is to contrast the same chemical system (Ga,In)N on (001) GaN substrate to the other two thermodynamic situations: bulk-incoherent and bulk-coherent alloys.

The epitaxial strain energy $U^{\text{epi}}(\sigma,a_{\text{sub}})$ is defined as the energy change when biaxially deforming structure σ from its equilibrium state to sharing the same lattice constant as substrate a_{sub} in the substrate plane. The constrained total energy $E^{(c)}(\sigma)$ [Eq. (2)] of structure σ is therefore $E^{(c)}(\sigma)=E(\sigma)+U^{\text{epi}}(\sigma,a_{\text{sub}})$. Similarly, the constrained total energy of the two constituents is

$$E^{(c)}(AC+BC) = (1-x)[E_{AC}(a_{AC}) + U_{AC}^{\text{epi}}(a_{\text{sub}})] + x[E_{BC}(a_{BC}) + U_{BC}^{\text{epi}}(a_{\text{sub}})]. \tag{7}$$

The formation enthalpy characterized by the excess energy of constrained system $\delta E(\sigma)$ [Eq. (2)] can then be expressed as

$$\Delta H^{\text{epi}}(\sigma) = \delta E^{\text{epi}}(\sigma) = \Delta E(\sigma,x) - [(1-x)U_{AC}^{\text{epi}}(a_{\text{sub}}) + xU_{BC}^{\text{epi}}(a_{\text{sub}}) - U^{\text{epi}}(\sigma,a_{\text{sub}})]. \tag{8}$$

The substrate is often chosen to have lattice constant between those of the pure constituents AC and BC. Consequently, the last term in Eq. (8) is usually positive. The epitaxial formation enthalpy $\Delta H^{\text{epi}}(\sigma)$ is thus reduced from $\Delta H_{\text{bulk}}^{\text{incoh}}(\sigma)$ [Eq. (3)] by a positive amount of energy. Figure 2 schematically shows the effect of epitaxial strain on the energetic order of various phases in an epitaxial thin film. It is seen that substrate coherence could induce a higher strain energy for AC and BC components than for the ordered configuration σ, i.e., $(1-x)U_{AC}^{\text{epi}}(a_{\text{sub}})+xU_{BC}^{\text{epi}}(a_{\text{sub}})>U^{\text{epi}}(\sigma,a_{\text{sub}})$, thus making the bulk-thermodynamic-unstable ordered compound σ epitaxially stable.

IV. METHODS OF CALCULATIONS

Here, we discuss how to calculate for a given alloy system the formation energies $\Delta E(\sigma)$ and $\delta E(\sigma)$, how to find the

lowest energy structures at $T=0$ and then how to compute the temperature-composition phase diagrams.

A. Calculations of the configurational energy and phase diagram for bulk-incoherent alloys

Since the configurational excess energy $\Delta E(\sigma)$ of Eq. (1) encompasses $O(2^N)$ configurations for a unit cell of N sites, direct first-principles calculations of all of these structures are practically impossible. We calculate, instead, O(50) structures with first-principles local-density approximation (LDA) and project the results on a generalized cluster expansion, allowing us to readily and accurately evaluate $O(2^N)$ structures. The excess energy $\Delta E(\sigma)$ [Eq. (1)] of (Ga,In)N pseudobinary zinc blende semiconductor alloy is described here by using a mixed-basis cluster expansion[18] (MBCE) total-energy Hamiltonian. Within the cluster expansion framework, one first chooses an underlying parent lattice (e.g., fcc for pseudobinary zinc blende alloys) and defines a configuration σ as a specific atomic occupation of each of the N lattice sites of parent lattice (e.g., fcc and bcc) by A or B atom (spin variable $s_i=-1$ or 1).

$$\Delta E_{CE}(\sigma) = J_0 + \frac{1}{N}\left[\sum_i J_i s_i + \sum_{i,j} J_{ij} s_i s_j + \sum_{i,j,k} J_{ijk} s_i s_j s_k + \cdots\right] + \sum_{\boldsymbol{k}} \Delta E_{CS}(\hat{\boldsymbol{k}},x) F(\boldsymbol{k},\sigma), \qquad (9)$$

where $J_{ij}, J_{ijk}, \ldots$ are the two-body, three-body, etc., interaction energies and $F(\boldsymbol{k},\sigma)=|S(\boldsymbol{k},\sigma)|^2 e^{-|\boldsymbol{k}|^2}/4x(1-x)$ is an attenuation term for short-concentration waves. The last term represents atomic size-mismatch effects, in which the *constituent strain energy* $\Delta E_{CS}(x,\hat{\boldsymbol{k}})$ is defined in Eq. (5).

All of the quantities that define the MBCE in Eq. (9) are determined by first-principles total-energy calculations. The interaction energies $\{J_{ij},\ldots\}$ are obtained by fitting of $\Delta E_{CE}(\sigma)$ to a set of first-principles calculated excess total energies $\{\Delta E_{\text{LDA}}(\sigma)\}$. The total energy are calculated with the local density approximation[20] and projected augmented wave (PAW) method, as implemented in Vienna ab initio simulation package (VASP) code.[21] The Brillouin zone was sampled with Monkhost–Pack k-point meshes with roughly constant mesh densities corresponding to $9\times 9\times 9$ for the fcc unit cell. The basis set cutoff energy is set as 435 eV. The error bounds on ΔE is about 1 meV/atom (thus, it is difficult to resolve structures with energy difference within this range). A leaving-many-out Cross-validation (CV) score[22] is adopted as a fitting quality parameter. The interactions are obtained by first eliminating from the fit several ordered structures and choosing the interactions that result in the best prediction error (i.e., the CV score) for the eliminated configurations. The process is repeated with including more LDA inputs until a desired accuracy is achieved.

Once the excess energy $\Delta E(\sigma)$ is cluster expanded, the exhaustive enumeration method[23] is adopted to calculate the energy for all $O(2^N)$ ordered structures σ with up to $N=20$ cations per unit cell (including about 2×10^6 configurations). In such an exhaustive enumeration method,[23] the configuration space is divided into different cell shapes and in each cell shape, an atomic configuration σ is obtained by decorating cation sublattice sites with an A or a B atom. Such an enumeration method gives us the energy of $O(2^{20})$ structures in Fig. 3(a). As for a random alloy, its energy is calculated by Monte Carlo simulations at a very high fictitious temperature (e.g., at temperature $T=10\,000$ K here) for which the correlation between lattice sites can be omitted.

We find for (Ga,In)N alloy that the formation energies $\Delta H_{\text{bulk}}^{\text{incoh}}(\sigma)$ of both ordered structures ($N\leq 20$) and random alloy are positive (see below). In terms of classical metallurgy,[13] this is a phase-separation system and its composition-temperature phase diagram is characterized by a "miscibility gap," under which it phase separates into InN-rich and GaN-rich solid solutions. To calculate such a miscibility gap, we need to integrate the Gibbs free energy $G(x,T)$ of the solid solution phase, $G(x,T)=\Delta H(x,T)-TS(x,T)$, where $S(x,T)$ is the mixing entropy of a solid solution of $Ga_{1-x}In_xN$ at composition x and temperature T. The heat capacity C_V can be related to mixing entropy through $C_V(x,T)=T[\partial S(x,T)/\partial T]$. $S(x,T)$ can, therefore, be integrated as

$$S(x,T) = S(x,T_0) + \int_{T_0}^{T} \frac{C_V(x,T)}{T} dT. \qquad (10)$$

The starting point T_0 is chosen as a very high temperature of 10 000 K, at which the ideal mixing entropy is a good approximation,

$$S(x,T_0=10\,000) \approx -k_B[x\ln(x) + (1-x)\ln(1-x)]. \qquad (11)$$

Both the formation enthalpy $\Delta H(x,T)$ and the heat capacity $C_V(x,T)$ can be calculated in a canonical Monte-Carlo simulation by using the cluster expansion [Eq. (9)] as energy functional. The free energy $G(x,T)$ can then be integrated. The miscibility gap is determined by the well-known "common-tangent line" approach. The spinodal decomposition line is calculated by searching the composition wherein the second partial differential of free energy $G(x,T)$ with respect to composition x equals zero at a given temperature T.

B. Calculations of the configurational energies and phase-diagram for bulk-coherent alloys

We describe the excess energy $\Delta E(\sigma)$ in Eq. (6) by using the mixed basis cluster expansion method [Eq. (9)], as described in Sec. III. It turns out that the $\Delta E_{CS}(\hat{\boldsymbol{k}},x)$ term reaches the lowest value at $\hat{\boldsymbol{k}}$ along the (001) direction for typical III-V semiconductor alloys.[12,15] Formation enthalpy $\Delta H_{\text{bulk}}^{\text{coh}}$ is therefore

$$\Delta H_{\text{bulk}}^{\text{coh}}(\sigma) = \Delta E_{CE}(\sigma,x) - \Delta E_{CS}(\hat{\boldsymbol{k}}_{(001)},x). \qquad (12)$$

As shown in Fig. 1, the lattice coherence strain energy $\Delta E_{CS}^{\text{min}}$ leads to the negative formation enthalpy $\Delta H_{\text{bulk}}^{\text{coh}}(\sigma)$ of certain configurations. At a low temperature, the bulk-coherent alloy system exhibits an ordering behavior instead of phase separation in the bulk-incoherent alloy. Usually, its

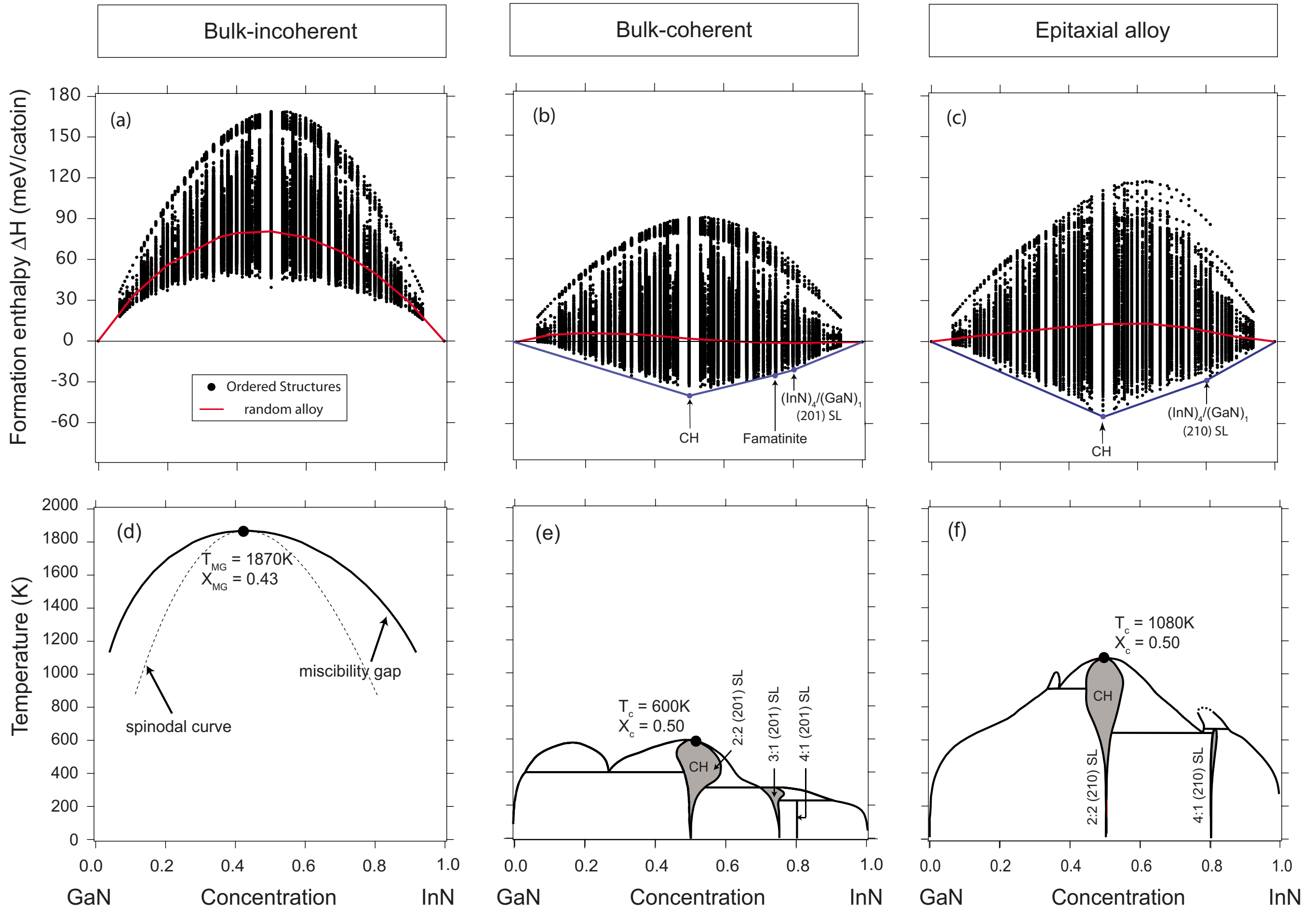

FIG. 3. (Color online) Formation enthalpies and phase diagrams of zinc blende (Ga,In)N semiconductor alloy under three thermodynamic states: (a, d) bulk-incoherent thermodynamics, (b, e) bulk-coherent thermodynamics and (c, f) substrate-coherent-epitaxial thermodynamics on (001) GaN substrate. In bulk-coherent alloys (b), three (201) superlattice (SL) structure chalcopyrite(CH) $(InN)_2/(GaN)_2$, famatinite $(InN)_3/(GaN)_1$ and $(InN)_4/(GaN)_1$ are predicted to the ground states. For substrate-coherent-epitaxial alloy, two (210) superlattices chalcopyrite $(InN)_2/(GaN)_2$ and $(InN)_4/(GaN)_1$ are predicted to be ground state structures.

phase diagram has richer features than the miscibility-gap. The free energy integration approach described above, for every candidate phase is not feasible any more. The phase boundary tracing algorithm developed by van de Walle *et al.*[24] and implemented in the ATAT software package[25] is employed here to construct the whole phase diagram. This method is coupled with semigrand-canonical ensemble Monte Carlo simulation. In a semigrand-canonical ensemble, the phase transition occurs when two phases have the same natural thermodynamic potential (free energy). Once we have found a transition point (on phase boundary), it decides the change in chemical potential with respect to the temperature change to preserve the equality of the free energies between those two phases and then calculates the concentrations of the two phases at this updated chemical potential and temperature via the semigrand-canonical Monte Carlo simulations. We obtain the whole phase boundary by scanning temperature T upward or downward.

C. Calculations of configurational energies and phase-diagram of substrate-coherent epitaxial alloys

The epitaxial strain energy $U^{\mathrm{epi}}(\sigma)$ [Eqs. (7) and (8)] is a function of atomic configurations as the excess energy [Eq. (1)]. However, each structure may now have more than one epitaxial strain energy, depending on its relative orientation with respect to the substrate. Let us consider, for example, a zinc blende GaN (001) substrate on which one places an ordered structure $(InN)_1/(GaN)_1$ ($L1_0$, or called CuAu-I type). $L1_0$ is a superlattice structure composed of alternate atomic monolayers along the (100)-equivalent crystallographic directions. It has three different variants: variant I is the $L1_0$ structure with periodicity along (100) direction, variant II is the one with periodicity along (010), variant III is with periodicity along the (001) direction. In the absence of a substrate, these three variants are symmetry equivalent and, thus, the excess energy cluster expansion [Eq. (9)] does not distinguish them. However, the epitaxial strain energies of these three structures on a GaN (001) substrate are obviously different. A principle requirement in cluster expansion is that the physical properties we cluster expand must have a one-to-one mapping to the configuration σ. We have developed a new cluster expansion[26] for the formation enthalpy $\Delta H^{\mathrm{epi}}(\sigma)$ [Eq. (8)] in the epitaxial alloy system. The underlying parent lattice is chosen as a tetragonal lattice, i.e., an elongated fcc lattice along the (001) substrate direction, so that it is capable of distinguishing the three variants of $L1_0$ epitaxial struc-

tures. The details of this epitaxial cluster expansion will be presented in another publication.[26] All of the interaction energies are determined by fitting to first-principles calculations for a set of ordered structures, using the local density approximation[20] and ultrasoft pseudo-potential, as implemented in VASP code.[21] The leaving-many-out CV score[22] is adopted as a fitting quality parameter. Once the best cluster expansion is determined for a given set of LDA input, we use this cluster expansion to predict the ground state structures, then calculate the LDA energies of the newly predicted ground states, and input them into next fitting iteration. This process is repeated until the ground state structures predicted by our cluster expansion agree with the LDA calculations and a desired accuracy is reached.

We calculated the formation enthalpy $\Delta H^{epi}(\sigma)$ for configurations with less than 16 cations per unit cell by the exhaustive enumeration method. Because formation enthalpies $\Delta H^{epi}(\sigma)$ are negative for certain structures, a (Ga,In)N thin film on a GaN (001) substrate is also an ordering system. The ATAT code[24,25] is adopted to calculate the phase diagram.

Teles *et al.*[27] adopted a real space cluster expansion assuming fcc parent lattice to describe the epitaxial phases of (Ga,In)N zinc blende alloys on a GaN (001) substrate. As we described above, such approach assuming fcc parent lattice cannot distinguish the different epitaxial variants that have different orientations with respect to the substrate. Teles *et al.*[27] thus expanded the average energy of the three different orientations. Due to such a limitation, Teles *et al.*[27] provided only a qualitative study of the epitaxial strain induced ordering in epitaxial thin films.

V. RESULTS

Figure 3 shows the formation enthalpies $\Delta H(\sigma)$ and the composition-temperature phase diagrams of (Ga,In)N cubic zinc blende alloy under the three thermodynamic states: bulk-incoherent alloy [Figs. 3(a) and 3(d)], bulk-coherent alloy [Figs. 3(b) and 3(e)], and substrate-coherent epitaxial alloy [Figs. 3(c) and 3(f)].

A. Bulk-Incoherent (Ga,In)N alloy: Formation enthalpies and phase diagram

Figure 3(a) shows the formation enthalpy $\Delta H^{incoh}_{bulk}(\sigma)$ for all ordered structures with up to 20 cations per unit cell and for the random alloy. They are all positive. The miscibility gap is shown in Fig. 3(d) with the transition temperature as T_{MG}=1870 K. The miscibility gap of bulk-incoherent (Ga,In)N alloy was previously calculated by different energy models, e.g., by valence-force-filed[28,29] and first-principles calculations.[30,31] The transition temperature T_{MG} obtained was in the range of 1400–2200 K. This large variance can be attributed to the usage of different energy and statistical models that are summarized in Table I. Gan *et al.*[30] approximated the random alloy energy by the energy of spatial-quasirandom-structure[32] obtained by first-principles calculations and adopted the regular solution model to determine the transition temperature T_{MG}: i.e., 2231 K (zinc blende) and 2132 K (wurtzite). Burton *et al.*[31] used the first-principles calculations and real space cluster expansion (around 30 LDA inputs and ten pair interactions) to describe the energy functional and employed the grand-canonical Monte Carlo simulations to obtain the phase diagram. The transition temperature is calculated as 1850 K (wurtzite).[31] Our result is close to these first-principles calculations. In our calculations, the statistics of atomic swapping is fully accounted via the Monte Carlo simulations, while the lattice vibration contribution is not included. It is known that, generally, the solid solution has a higher entropy S_{vib} from lattice vibration than ordered structure and separated phases.[33] The solid solution phase is stabilized by S_{vib} and, consequently, has a lower calculated transition temperature. In Refs. 30 and 31, it is found that lattice vibration can reduce the transition temperature about 200–450 K for zinc blende and wurtzite (Ga,In)N alloy. We expect our calculated transition temperature could drop by a similar amount if we take lattice vibration into consideration.

For semiconductor alloys, the bulk-incoherent thermodynamic state applies for the thick bulk film above the critical thickness,[19] defects are well developed, allowing the crystal lattice to relax. In the case of (Ga,In)N alloys, phase separation is very often observed for both zinc blende alloys[34–36] grown on a GaAs (001) substrate by MBE and wurtzite alloys grown on a sapphire (0001) substrate by MBE or MOCVD.[37–43] In most of these experiments, alloys with an In concentration above 20% exhibit phase separation at the typical growth temperature of around 1000–1200 K. Such experimental measured composition-temperature window very well agrees with our calculated spinodal curve [Fig. 3(d)].

B. Bulk-coherent (Ga,In)N alloy: Ground state structures and phase diagram

The prediction of ground state structures is done in two steps: First, one searches the lowest energy configurations $\sigma_{min}(x_i)$ from many alternative configurations at concentration x_i [based on Eqs. (12) and (9)]. This gives the "lowest energy structure at a fixed x" (LESFX). Second, one examines if $\sigma_{min}(x_i)$ is stable with respect to disproportion into two configurations at neighboring compositions x_{i+1} and x_{i-1}. This step involves the construction of a *convex* hull of $E[\sigma_{min}(x_i)]$ vs x. In this step, many LESFX are eliminated as ground state structures. Note that in a thermodynamic phase-diagram, LESFX do not appear but only the ground state structures do. Figure 3(b) shows that for bulk-coherent (Ga,In)N, there are three "breaking points" (i.e., the ground state structures) in the convex hull, resulting from searching 2^{20} possible configurations whose energies are given by the cluster expansion $\Delta H^{coh}_{bulk,CE}(\sigma)$ [Eq. (12)]: (i) the 2:2 structure $(InN)_2/(GaN)_2$ chalcopyrite (CH) at x=0.50, (ii) the 3:1 structure $(InN)_3/(GaN)_1$ famatinite (FM) at x=0.75, and (iii) the 4:1 structure $(InN)_4/(GaN)_1$ at x=0.80. All of these ground state structures are short-period superlattices along the (201) crystal direction.

A ground state search requires knowledge of the energies of a large number of configurations (here, $\sim 2^{20}$) for other-

TABLE I. Comparison of the miscibility gap transition temperatures T_{MG} calculated for wurtzite (WZ) and zinc blende (ZB) (Ga,In)N alloys by different energy and statistical models. Here, FP stands for first-principles calculations, CE stands for cluster expansion, SQS stands for the spatial quasirandom structure (Ref. 32), VFF stands for valence-force-field model, RSM stands for regular solution model, where the mixing entropy is approximated by ideal mixing, and DLP stands for the delta-lattice-parameter model.

References	Energy functional	Statistics	Lattice vibration	T_{MG} (K) (WZ)	T_{MG} (K) (ZB)
Present work	FP+MBCE	Monte Carlo	No		1870
Burton *et al.*[a]	FP+CE	Monte Carlo	No	1850	
			Yes	1620	
Gan *et al.*[b]	FP+SQS	RSM	No	2132	2231
			Yes	1654	1771
Ferhat *et al.*[c]	FP+64 atom supercell	RSM	No	1400	
Ho *et al.*[d]	VFF	DLP	No	1523	
Adhikari *et al.*[e]	VFF	Monte Carlo	No	1500	
Takayama *et al.*[f]	VFF	RSM	No	1967	1668
Saito *et al.*[g]	VFF	RSM	No	1690	
Purton *et al.*[h]	Ionic potential	Monte Carlo	Yes	1725	1725
Karpov *et al.*[i]	VFF	RSM	No		1818
	VFF	Numerical evaluation of partition function	No		1906

[a]Reference 31.
[b]Reference 30.
[c]Reference 75.
[d]Reference 28.
[e]Reference 76.
[f]Reference 77 and 78.
[g]Reference 79.
[h]Reference 80.
[i]Reference 81.

wise one might incorrectly identify a ground state structure. For example, Fig. 3(b) shows that whereas the In-rich $In_{0.75}Ga_{0.25}N$ composition has a stable coherent ground state, the symmetric counterpart $In_{0.25}Ga_{0.75}N$ does not, for it will spontaneously disproportionate into a mixture of 50% $(InN)_2/(GaN)_2$ CH phase plus 50% pure GaN. This mixture has a lower energy than the lowest energy configuration of $(InN)_1/(GaN)_3$. The reason that In-rich $(InN)_3/(GaN)_1$ has systematically lower energy than Ga-rich $(InN)_1/(GaN)_3$ is a manifestation of the fact that the total energy vs volume curve is characteristically steeper at a lower volume than at a large volume, so it is easier to introduce a small atom (Ga) into a lattice containing a majority of large atoms (In) than the reverse. In the absence of an exhaustive search, one might be naively tempted to calculate the energies of different configurations of $InGa_3N_4$, i.e., LESFX, confusing these with the ground state structures. Similarly, without an exhaustive search, unsuspected ground states, such as the $(InN)_4/(GaN)_1$ (201) superlattice, might be missed.

1. Ground state structure of bulk coherent $In_{0.75}Ga_{0.25}N$

Our search of many possible configurations from $\{\Delta H^{coh}_{bulk,CE}(\sigma)\}$ [Eq. (12)] revealed a ground state structure at this composition for the famatinite $(InN)_3/(GaN)_1$ (201) superlattice structure, with another (201) superlattice $(GaN)_1/(InN)_2/(GaN)_1/(InN)_4$ (201) (called Q8) as an excited-state configuration with an energy of 0.9 meV/atom higher. Such a small difference is difficult to resolve, as it is within the range of uncertainty of our cluster expansion. Indeed, Wei *et al.*[44] found in direct calculations of ΔH that, although the VFF energy functional does predict FM to be lower than Q8 (by 0.3 meV/atom), the generalized gradient approximation–PAW predicts a reverse energy order with Q8 being 0.3 meV/atom lower than FM. Our LDA-USPP and LDA-PAW calculations also confirmed that the Q8 has an energy of about 0.6 meV/atom lower than FM. Thus, $\Delta H^{coh}_{bulk,CE}(\sigma)$ and $\Delta H_{bulk,LDA}(\sigma)$ was different by $\lesssim 1$ meV/atom. The precise ground state at $x=0.75$ for $In_{0.75}Ga_{0.25}N$ is too close to call (note that the error of our first-principles calculations is about 1 meV/atom), although we are certain that there is a single-composition ground state (unlike the phase-separation predicted at $x=0.25$) and that it corresponds to 3:1 InN:GaN with (201) ordering.

Inspection of Fig. 3(b) reveals not only the pronounced asymmetry, whereby In-rich compounds are asymmetrically lower in energy than Ga-rich, but also that many of the In-rich compounds lie very close to the ground state line with a negligible excitation energy. In fact, there is a quasicontinuum of In-rich compounds that are nearly ground states. This phenomenon is called "adaptive structures."[45] Examin-

ing the crystal structures at those compositions shows that all of them are (201) superlattices. We conclude that in In-rich domain, there are quasidegenerate adaptive structures that differ from each other by small structural mutations.

2. Absence of ground state structure of bulk coherent $In_{0.25}Ga_{0.75}N$

Our CE predicts no "breaking point" at this composition. The reason is that $\Delta H^{\rm coh}_{{\rm bulk},CE}(\sigma)$ of two phase mixture of 50% $(InN)_2/(GaN)_2$ (201) plus 50% GaN is 1.72 meV/atom *lower* than the lowest energy of the ordered structure $(InN)_1/(GaN)_3$. Our direct first-principles calculations $\Delta H^{\rm coh}_{\rm bulk,LDA}(\sigma)$ show that the mixture of CH and GaN has indeed an energy 2 meV/atom lower than the lowest energy structure at $x=0.25$. VFF calculations confirm this observation. It is worth noting here that our definition of coherent energy in Eq. (6) involves the subtraction of a composition-dependent function $\Delta E^{\rm min}_{CS}(x)$ from bulk-coherent energy $\Delta H^{\rm incoh}_{\rm bulk}(\sigma)$ of Eq. (3). Thus, inspection of $\Delta H^{\rm incoh}_{\rm bulk}(\sigma)$ is not sufficient to draw the ground state line of coherent structures. This is evident from the comparison of Figs. 3(a) and 3(b).

3. Trends among different anions for bulk-coherent structures

It is interesting to enquire if different anion X in (Ga, In)X or even different III-V alloys universally produce the same coherent ground state structure or not. This issue was previously addressed in Refs. 17 and 46.

(i) By using direct LDA calculations for $\Delta H^{\rm coh}_{\rm bulk,LDA}(\sigma_{\rm input})$ and a simplified $\varepsilon - G$ method for the cluster expansion $\Delta H^{\rm coh}_{{\rm LDA},CE}(\sigma)$, Wei *et al.*[17] found for Ga(As, Sb), (Ga, In)P, (Ga, In)As, (Hg, Zn)Te, and (Cd, Zn)Te the universal ground state structures: (a) $(AC)_2/(BC)_2$ (201) superlattice (CH), (b) $(AC)_1/(BC)_2/(AC)_1/(BC)_4$ (201) superlattice (Q8), and (c) $(AC)_1/(BC)_4$ (201) superlattice.

(ii) A mixed basis cluster expansion fitted by direct LDA calculations for a set of $\{\sigma_{\rm input}\}$ gave Lu *et al.*[46] CH as the bulk-coherent ground state structure for (Ga, In)P at $x=0.50$. However, at $x=0.75$, Lu *et al.*[46] found a 16-cation structure (Q16) as the ground state.

(iii) Our direct VFF minimization (no CE) for $\sim 2^{20}$ structures of (In, Ga)N, (In, Ga)P, (In, Ga)As, (In, Ga)Sb, In(As, P), and In(As, Sb) predicts that at $x=0.50$ and $x=0.80$, CH and the $(AC)_1/(BC)_4$ (201) superlattice are universally the ground state structures. However, at $x=0.75$, FM is the ground state for (In, Ga)N, Q8 is the ground state for In(As, P) and In(As, Sb), and a 20-cation structure (Q20) is the ground state for (In, Ga)P, (In, Ga)As, and (In, Ga)Sb alloys. Direct LDA calculations are not able to scan sufficient structures to determine a ground state line. Instead, lowest energy structures at fixed compositions are determined. Within computational accuracies, mixed-cation systems at $x=0.75$ produce degenerate structures.

In summary, at $x=0.50$ and $x=0.80$, CH and the $(AC)_1/(BC)_4$ (201) superlattice are the universal ground state structures, while at $x=0.75$, it appears that there is a delicate competition between FM, Q8, Q16, and Q20 and no universal ground state structure emerges.

4. Finite temperature phase diagram for bulk-coherent alloys

Figure 3(e) shows the calculated bulk-coherent phase diagram. The order-disorder transition temperature at $x=0.5$ is around $T_c=600$ K, which is only about 1/3 of the miscibility gap transition temperature, $T_{\rm MG}=1870$ K, for the bulk-incoherent state. The transition temperatures at $x=0.75$ and $x=0.80$ are calculated as 310 and 235 K.

The bulk-coherent state applies to thick films above the critical thickness. Additionally, high crystal quality is required (i.e., very few dislocations and grain boundaries to damage the crystal coherence). It would be difficult to achieve such requirements during the thick film growth, especially for an $In_xGa_{1-x}N$ alloy, wherein the large lattice mismatch ($\sim$11%) leads to a high density of dislocations $\sim 10^9/{\rm cm}^{-2}$ inside the sample. Great care must be taken during growth in experiments. The (201) chalcopyrite ordering has been seen as nanometer size precipitates ($\leq$50 nm) in the bulk sample for some zinc blende alloy systems, such as (Ga, In)As (Ref. 47) and Ga(As, Sb).[48] Since the natural form of an $In_xGa_{1-x}N$ alloy is the wurtzite structure, there are only a few experimental results for the bulk-coherent zinc blende alloys. We are not aware of any report of ordering structures in the cubic zinc blende (Ga,In)N system. However, for bulk wurtzite (Ga,In)N alloys, ordered precipitates with a nanometer size at about $x=0.50$ were observed[38,42,43,49] in thick films grown on sapphire (0001) substrates, wherein the transmission electron microscopy selected area diffraction patterns demonstrate the ordering as an alternative monolayer stacking of In and Ga atoms along the c-direction. The bulk-coherent thermodynamic state provides a qualitative explanation for understanding the formation of such ordered structures.

For a zinc blende (Ga,In)N bulk alloy, the optimal thermodynamic condition for the formation of the predicted ordered CH structure is at $x=0.50$ because the thermodynamic driving force (i.e., the free energy difference) for a disorder-order transformation is maximal at this concentration. Annealing is also required because the calculated transition temperature $T_c=600$ K is below the typical growth temperature of 1000–1200 K in experiments. Care should also be taken during the annealing to avoid generation and development of defects, such as misfit dislocations, and grain boundaries.

C. Substrate-coherent epitaxial (Ga,In)N alloy

Figure 3(c) shows the formation enthalpy $\Delta H^{\rm epi}(\sigma)$ of $O(2^{16})$ configurations and the random alloy for a (Ga,In)N epitaxial thin film coherently grown on a GaN (001) substrate. The ground state convex hull is represented by the solid line, in which the breaking points are the ground state structures: the chalcopyrite $(InN)_2/(GaN)_2$ superlattice along the (210) direction (at $x=0.5$) and the $(InN)_4/(GaN)_1$ superlattice along the (210) direction (at $x=0.8$). It is worth noting that the counterparts of these two structures along the (201) crystal direction are not ground states.

The phase diagram is illustrated as Fig. 3(f). At $x=0.5$, the order-disorder transition temperature is determined as around 1080 K, which is about one-half of the miscibility-gap tem-

perature $T_{MG}=1870$ K of the bulk-incoherent state but is much higher than the transition temperature $T_c=600$ K of the bulk-coherent state. The transition point at $x=0.80$ is calculated as around 630 K.

The effect of epitaxial strain on the thermodynamics of (Ga,In)N alloys is discussed in Refs. 27, 29, and 50. Teles *et al.*[27] used their real space cluster expansion for "averaged energy" (see Sec. IV C) to obtain the "ground states" as chalcopyrite (at $x=0.50$) and the $(InN)_3/(GaN)_1/(InN)_2/(GaN)_2$ (201) superlattice (at $x=0.625$). They qualitatively predicted the substrate-coherence induced ordering in such alloys, but the obtained ground states are not the true ground states as we have discussed in this paper. The composition-temperature phase diagrams for (Ga,In)N epitaxial thin films on substrate were calculated by Karpov *et al.*[29] and Teles *et al.*[50] Both calculations failed to predict substrate-coherent induced ordering because their treatments of epitaxial strain were insufficient. This is because they[29,50] adopted much simpler energy functionals to take epitaxial strain into account and employed simple statistical models (e.g., regular solution and quasichemical approximation) to calculate the phase diagrams.

In discussing the thermodynamic properties of substrate-coherent epitaxial alloys, we assume a perfect registry of the thin film to the substrate. Theoretically, this is valid when thin film thickness is below the critical value h_c.[19] The critical thickness is a function of the lattice mismatch between the alloy and the substrate. For the interesting application of $In_xGa_{1-x}N$ alloys with $x\sim0.10-0.30$ for blue or green light emission diode (LED), the calculated critical thickness is below 30 nm. Thus, the substrate-coherent alloy thermodynamics applies for quantum well (QW) devices. We can use our calculated phase diagram to analyze the controversy about the atomic microstructures in such a QW.[36,51–56]

In spite of the high dislocation density and the strong internal built-in piezoelectric field, blue LED devices with InGaN alloys with an In concentration of $\sim0.10-0.30$ as the active material have a surprisingly high internal quantum efficiency. Chichibu *et al.*[57] attributed this to the recombination of excitons at certain potential local minima. Subsequently, numerous models were proposed to explain this localization from the aspect of the composition inhomogeneity, such as the presence of composition fluctuation in the alloy,[57–59] quantum dot structures with an In concentration of $\sim0.40-0.60$ (Refs. 60–70), and even nearly pure InN.[53,68,71] However, Smeeton *et al.*[54] recently pointed out that the observed quantum-dot-like structures in the QW samples[58,68] might be due to electron beam damage. Li *et al.*[72] observed that the calculated In concentration in the clusters [evaluated by lattice-fringe high resolution transmission electron microscopy (HRTEM) images and by assuming Vegard's law] increased with increasing irradiation time in the electron microscope. Galtrey *et al.*[73] used a three dimensional atom probe technique to reconstruct the three-dimensional atom map of the active region of the QW and no such quantum dot structures were observed in their samples. Lai *et al.*,[65] however, found quantum dot structures with an In concentration $x=0.54-0.59$ even if they did careful measurement to avoid the possible electron beam damage.

Phase separation for the bulk-incoherent (Ga,In)N alloy[28] [Fig. 3(d)] was often taken for granted to support the presence of the quantum dot microstructures in the quantum well.[53,58,68,71,74] As we have shown in this paper, the quantum well devices have completely different thermodynamics due to the presence of the substrate. In Fig. 3(e), at a typical growth temperature of $\sim1000-1200$ K and an In composition $x\sim0.10-0.30$, the solid solution phase is thermodynamically stable and, thus, there is no phase separation. If we assumed the inhibited kinetics for thin quantum well devices during cooling from the growth temperature, there would be no quantum dots and strong composition fluctuation at room temperature, as proposed in Refs. 55 and 73. However, if the atomic diffusion is not completely inhibited during the cooling, the formation of precipitates at about $x=0.50$ (Refs. 60–70) or the composition fluctuation[57,58,72] is still thermodynamically possible. Thus, our calculation predicts no nearly pure InN quantum dots in the QW devices,[53,68,71] while random alloys,[55,73] composition fluctuation,[57–59] and the formation of quantum dot structures close to $x=0.50$ (Refs. 60–70) are possible.

The optimal thermodynamic condition for the formation of the predicted ordered structure CH-(210) occurs at $x=0.50$ because the thermodynamic driving force for disorder-order phase transition is maximal at this concentration. Additionally, the lattice constant of the substrate should be close to those of the solid solution $In_{0.5}Ga_{0.5}N$ and the CH-(210) in order to increase the critical thickness h_c. The alloy film, therefore, can be grown thick enough so that its thickness would not interfere with the formation of the ordered CH-(210) structure.

VI. SUMMARY

We have discussed the thermodynamic properties of a semiconductor alloy in three different thermodynamic states for different semiconductor growth modes: bulk-incoherent, bulk-coherent, and substrate-coherent epitaxial thermodynamics. The summary of the conditions defining these three states are listed in Table II.

(1) *Bulk-incoherent alloys*: Due to the large lattice mismatch between the two constituents *AC* and *BC*, the bulk-incoherent alloy has a positive formation enthalpy $\Delta H^{\mathrm{incoh}}_{\mathrm{bulk}}(\sigma)$ [Fig. 3(a)]. Consequently, we obtain the characteristic "miscibility gap" in the composition-temperature phase diagram [Fig. 3(d)], below which the alloy incoherently phase separates into *AC*-rich and *BC*-rich solutions. The transition temperature is calculated as $T_{MG}=1870$ K for zinc blende (Ga,In)N alloy. This thermodynamic state applies for a thick bulk film above the critical thickness with a high density of dislocations relaxing the crystal lattice coherence.

(2) *Bulk-coherent alloys*: When crystal lattice coherence is maintained before and after phase transformation, the strain energy $\Delta E^{\mathrm{min}}_{CS}(x)$ cost to maintain the lattice coherence destabilizes the constituent phase separation [Fig. 1]. Consequently, the formation enthalpy $\Delta H^{\mathrm{coh}}_{\mathrm{bulk}}(\sigma)$ is reduced and becomes negative [Figs. 1 and 3(b)]. We found three (201) superlattice structures as the ground states: chalcopyrite $(InN)_2/(GaN)_2$ (201) at $x=0.50$, $(InN)_4/(GaN)_1$ at $x=0.80$, whereas at $x=0.75$ it is Q8 or FM. Figure 3(f) shows the

TABLE II. Summary of the three thermodynamic states for semiconductor alloys: bulk-incoherent thermodynamics, bulk-coherent thermodynamics, and substrate-coherent-epitaxial thermodynamics. The formation enthalpies $\Delta H(\sigma)$, ground state structures, methods adopted to calculate phase diagram, and the applications in experiments are listed for comparison.

	Bulk-incoherent thermodynamics	Bulk-coherent thermodynamics	Substrate-coherent epitaxial thermodynamics
Formation Enthalpy	$\Delta H^{\mathrm{incoh}}_{\mathrm{bulk}}(\sigma)=\Delta E(\sigma)$	$\Delta H^{\mathrm{coh}}_{\mathrm{bulk}}(\sigma)=\Delta E(\sigma)-\Delta E^{\mathrm{min}}_{CS}(x)$	$\Delta H^{\mathrm{epi}}(\sigma)=\Delta E(\sigma)-[(1-x)U^{\mathrm{epi}}_{AC}(a_{\mathrm{sub}})+xU^{\mathrm{epi}}_{BC}(a_{\mathrm{sub}})-U^{\mathrm{epi}}(\sigma,a_{\mathrm{sub}})]$
Ground states	Phase separation InN+GaN	CH $(\mathrm{InN})_2/(\mathrm{GaN})_2$ (201) SL FM $(\mathrm{InN})_3/(\mathrm{GaN})_1$ or Q8 (201) SL $(\mathrm{InN})_4/(\mathrm{GaN})_1$ (201) SL	CH $(\mathrm{InN})_2/(\mathrm{GaN})_2$ (210) SL $(\mathrm{InN})_4/(\mathrm{GaN})_1$ (210) SL
Phase diagram calculation	Canonical Monte Carlo; Common-tangent-line	Semigrand-canonical Monte Carlo; phase boundary tracing algorithm[a]	Semigrand-canonical Monte Carlo; phase boundary tracing algorithm[a]
Pertinent experiments	thick film ($>h_c$); without lattice coherence	Thick film ($>h_c$); with lattice coherence	Thin film ($<h_c$);

[a]Reference 25.

calculated phase diagram. The order-disorder transition temperature at $x=0.50$ is drastically reduced to $T_c=600$ K in comparison to the $T_{\mathrm{MG}}=1870$ K of bulk-incoherent state. This bulk-coherent thermodynamics applies for thick films above the critical thickness while keeping its crystal coherence (i.e., very few defects to damage the crystal coherence). It can serve as a new mechanism to understand the formation of chalcopyrite ordered structures in InAs-GaAs (Ref. 47) and GaAs-GaSb (Ref. 48) alloys and the ordering at $x=0.5$ in wurtzite (Ga,In)N thick bulk films.[38,42,43,49]

(3) *Substrate-coherent epitaxial alloys* (e.g., thin films with thickness $<h_c$): This alloy maintains a coherent registry to the substrate. The coherent strain from the substrate increases the energy of phase separation into substrate-coherent constituents (AC on substrate) and (BC on substrate) (Fig. 2) and, thus, the formation enthalpy $\Delta H^{\mathrm{epi}}(\sigma)$ becomes negative [Fig. 3(c)]. The ground state structures are found to be two (210) superlattices: the chalcopyrite $(\mathrm{InN})_2/(\mathrm{GaN})_2$ at $x=0.50$ and the $(\mathrm{InN})_4/(\mathrm{GaN})_1$ at $x=0.80$. Figure 3(e) shows the calculated phase diagram, and the order-disorder transition temperature at $x=0.50$ is determined to be around 1000 K, which is only about one-half of the transition temperature $T_{\mathrm{MG}}=1870$ K for the bulk-incoherent state (i.e., the traditional bulk alloy) but is much higher than $T_c=600$ K for the bulk-coherent state. This substrate-coherent-epitaxy thermodynamics applies for thin films below the critical thickness h_c. As an application, our theoretical result [Fig. 3(f)] shows that there is no theoretical evidence to support the formation of a nearly pure InN QD structure[53,68,71] in the QW, but supports that a random alloy;[55,73] the composition fluctuation[57–59] and quantum dots with an In composition of around 0.50 (Refs. 60–70) are thermodynamically possible.

ACKNOWLEDGMENTS

This research was funded by the U.S. Department of Energy, Office of Science, Basic Energy Sciences, Materials Sciences and Engineering, under Contract No. DE-AC36-99GO10337 to NREL, and the LDRD project from NREL. The authors thank S.-H. Wei for valuable discussions about the universal coherent ground states.

[1] A. Zunger and S. Mahajan, in *Handbook on Semiconductors*, edited by T. S. Moss (North-Holland, Amsterdam, 1992), Vol. 3, Pt. B, p. 1399.
[2] A.-B. Chen and A. Sher, *Semiconducotor Alloys* (Plenum, New York, 1995).
[3] A. Chin, A. Ourmazd, and E. M. Monberg, Appl. Phys. Lett. **58**, 968 (1991).
[4] G.-B. Stringfellow, *Organometallic Vapor-Phase Epitaxy: Theory and Practice* (Academic, San Diego, 1999).
[5] A. Zunger and D. M. Wood, J. Cryst. Growth **98**, 1 (1989).
[6] D. M. Wood and A. Zunger, Phys. Rev. B **40**, 4062 (1989).
[7] G. B. Stringfellow, J. Cryst. Growth **27**, 21 (1974).
[8] P. C. Kelires and J. Tersoff, Phys. Rev. Lett. **63**, 1164 (1989).
[9] James E. Bernard, S. Froyen, and Alex Zunger, Phys. Rev. B **44**, 11178 (1991).
[10] D. M. Wood and A. Zunger, Phys. Rev. Lett. **61**, 1501 (1988).
[11] Akiko Gomyo, Kikuo Makita, Isao Hino, and Tohru Suzuki, Phys. Rev. Lett. **72**, 673 (1994).
[12] J. Z. Liu, G. Trimarchi, and A. Zunger, Phys. Rev. Lett. **99**, 145501 (2007).
[13] D. A. Porter and K. E. Easterling, *Phase Transformations in Metals and Alloys* (Nelson Thornes, United Kingdom, 2001).
[14] Strictly, enthalpy $H(\sigma)=E(\sigma)+PV(\sigma)$, where P is pressure and V is volume. For semiconductor alloys under typical growth condition, the PV term is very small and, thus, it is assumed negligible.
[15] R. G. Dandrea, J. E. Bernard, S.-H. Wei, and A. Zunger, Phys. Rev. Lett. **64**, 36 (1990).

[16] L. G. Ferreira, S.-H. Wei, and A. Zunger, Phys. Rev. B **40**, 3197 (1989).
[17] S.-H. Wei, L. G. Ferreira, and A. Zunger, Phys. Rev. B **41**, 8240 (1990).
[18] David B. Laks, L. G. Ferreira, Sverre Froyen, and Alex Zunger, Phys. Rev. B **46**, 12587 (1992).
[19] J. W. Matthews and A. E. Blakeslee, J. Cryst. Growth **27**, 118 (1974).
[20] J. P. Perdew and Alex Zunger. Phys. Rev. B, **23**, 5048 (1981).
[21] G. Kresse and J. Furthmller, Comput. Mater. Sci. **6**, 15 (1996).
[22] The cross-validation score is calculated as the average prediction error for a given number of ordered structures by the cluster expansion that is least-squares fitted from the rest of configurations in a data pool.
[23] L. G. Ferreira, S.-H. Wei, and A. Zunger, Int. J. Supercomput. Appl. **5**, 34 (1991).
[24] A. van de Walle and M. Asta, Modell. Simul. Mater. Sci. Eng. **10**, 521 (2002).
[25] A. van de Walle (http://www.its.caltech.edu/ avdw/atat/).
[26] J. Z. Liu and A. Zunger (unpublished).
[27] L. K. Teles, L. G. Ferreira, L. M. R. Scolfaro, and J. R. Leite, Phys. Rev. B **69**, 245317 (2004).
[28] I. Ho and G. B. Stringfellow, Appl. Phys. Lett. **69**, 2701 (1996).
[29] S. Yu. Karpov, MRS Internet J. Nitride Semicond. Res. **3**, 1 (1998).
[30] C. K. Gan, Y. P. Feng, and D. J. Srolovitz, Phys. Rev. B **73**, 235214 (2006).
[31] B. P. Burton, A. van de Walle, and U. Kattner, J. Appl. Phys. **100**, 113528 (2006).
[32] A. Zunger, S.-H. Wei, L. G. Ferreira, and J. E. Bernard, Phys. Rev. Lett. **65**, 353 (1990).
[33] A. van de Walle and G. Ceder, Rev. Mod. Phys. **74**, 11 (2002).
[34] A. Tabata, J. R. Leite, A. P. Lima, E. Silveira, V. Lemos, T. Frey, D. J. As, D. Schikora, and K. Lischka, Appl. Phys. Lett. **75**, 1095 (1999).
[35] E. Silveira, A. Tabata, J. R. Leite, R. Trentin, V. Lemos, T. Frey, D. J. As, D. Schikora, and K. Lischka, Appl. Phys. Lett. **75**, 3602 (1999).
[36] V. Lemos, E. Silveira, J. R. Leite, A. Tabata, R. Trentin, L. M. R. Scolfaro, T. Frey, D. J. As, D. Schikora, and K. Lischka, Phys. Rev. Lett. **84**, 3666 (2000).
[37] R. Singh, D. Doppalapudi, and T. D. Moustakas, Appl. Phys. Lett. **70**, 1089 (1997).
[38] D. Doppalapudi, S. N. Basu, K. F. Ludwig, and T. D. Moustakas, J. Appl. Phys. **84**, 1389 (1998).
[39] N. A. El-Masry, E. L. Piner, S. X. Liu, and S. M. Bedair, Appl. Phys. Lett. **72**, 40 (1998).
[40] A. Wakahara, T. Tokuda, X.-Z. Dang, and S. Noda, Appl. Phys. Lett. **71**, 906 (1997).
[41] M. Rao, D. Kim, and S. Mahajan, Appl. Phys. Lett. **85**, 1961 (2004).
[42] M. Rao, N. Newman, and S. Mahajan, Scr. Mater. **56**, 33 (2007).
[43] M. K. Behbehani, E. L. Piner, S. X. Liu, N. A. El-Marsy, and S. M. Bedair, Appl. Phys. Lett. **75**, 2202 (1999).
[44] S. Chen, X. G. Gong, and S.-H. Wei, Phys. Rev. B **77**, 073305 (2008).
[45] M. Sanati, L. G. Wang, and A. Zunger, Phys. Rev. Lett. **90**, 045502 (2003).
[46] Z.-W. Lu, D. B. Laks, S.-H. Wei, and A. Zunger, Phys. Rev. B **50**, 6642 (1994).
[47] T. S. Kuan, W. I. Wang, and E. L. Wilkie, Appl. Phys. Lett. **51**, 51 (1987); N. Nakayama and H. Fujita, in *GaAs and Related Compounds 1985*, Institute of Physics Conference Series, edited by M. Fujimoto (Hilger, London, 1986), Vol. 79, p. 289.
[48] H. R. Jen, M. J. Cherng, and G. B. Stringfellow, Appl. Phys. Lett. **48**, 1603 (1986).
[49] P. Ruterana, G. Nouet, W. Van der Stricht, I. Moerman, and L. Considine, Appl. Phys. Lett. **72**, 1742 (1998).
[50] L. K. Teles, J. Furthmuller, L. M. R. Scolfaro, J. R. Leite, and F. Bechstedt, Phys. Rev. B **62**, 2475 (2000).
[51] S. F. Chichibu, A. Uedono, T. Onuma, B. A. Haskell, A. Chakraborty, T. Koyama, P. T. Fini, S. Keller, S. P. Denbaars, J. S. Speck, U. K. Mishra, S. Nakamura, S. Yamaguchi, S. Kamiyama, H. Amano, I. Akasaki, J. Han, and T. Sota, Nat. Mater. **5**, 810 (2006).
[52] S. F. Chichibu, A. Uedono, T. Onuma, B. A. Haskell, A. Chakraborty, T. Koyama, P. T. Fini, S. Keller, S. P. Denbaars, J. S. Speck, U. K. Mishra, S. Nakamura, S. Yamaguchi, S. Kamiyama, H. Amano, I. Akasaki, J. Han, and T. Sota, Philos. Mag. **87**, 2019 (2007).
[53] K. P. O'Donnell, R. W. Martin, and P. G. Middleton, Phys. Rev. Lett. **82**, 237 (1999).
[54] T. M. Smeeton, M. J. Kappers, J. S. Barnard, M. E. Vickers, and C. J. Humphreys, Appl. Phys. Lett. **83**, 5419 (2003).
[55] C. J. Humphreys, Philos. Mag. **87**, 1971 (2007).
[56] M. J. Galtrey, R. A. Oliver, M. J. Kappers, C. J. Humphreys, D. J. Stokes, P. H. Clifton, and A. Cerezo, Appl. Phys. Lett. **90**, 061903 (2007).
[57] S. Chichibu, T. Azuhata, T. Sota, and S. Nakamura, Appl. Phys. Lett. **69**, 4188 (1996).
[58] Y. Narukawa, Y. Kawahami, M. Funato, S. Fujita, S. Fujita, and S. Nakamura, Appl. Phys. Lett. **70**, 981 (1997).
[59] S. Nakamura, Science **281**, 956 (1998).
[60] K. Lischka, J. Cryst. Growth **231**, 415 (2001).
[61] O. Husberg, A. Khartchenko, D. J. As, H. Volgelsang, T. Frey, D. Schikora, K. Lischka, O. C. Noriega, A. Tabata, and J. R. Leite, Appl. Phys. Lett. **79**, 1243 (2001).
[62] A. Tabata, L. K. Teles, L. M. R. Scolfaro, J. R. Leite, A. Kharchenko, T. Frey, D. J. As, D. Schikora, K. Lischka, J. Furthmuller, and F. Bechstedt, Appl. Phys. Lett. **80**, 769 (2002).
[63] Y.-L. Lai, C.-P. Liu, and Z.-Q. Chen, Appl. Phys. Lett. **86**, 12915 (2005).
[64] II-Kyu Park, M.-K. Kwon, S.-H. Baek, Y.-W. Ok, Y.-S. Kim, Y.-T. Moon, and D.-J. Kim, Appl. Phys. Lett. **87**, 061906 (2005).
[65] Y.-L. Lai, C.-P. Liu, Y.-H. Lin, T.-H. Hsueh, R.-M. Lin, D.-Y. Lyu, Z.-X. Peng, and T.-Y. Lin, Nanotechnology **17**, 3734 (2006).
[66] M. D. McCluskey, L. T. Romano, B. S. Krusor, D. P. Bour, and S. Bernnan, Appl. Phys. Lett. **72**, 1730 (1998).
[67] L. T. Romano, M. D. McCluskey, B. S. Krusor, D. P. Bour, C. Chua, S. Brennan, and K. M. Yu, J. Cryst. Growth **189-190**, 33 (1998).
[68] P. Ruterana, S. Kret, A. Vivet, G. Maciejewski, and P. Dluzewski, J. Appl. Phys. **91**, 8979 (2002).
[69] D. Gerthsen, E. Hahn, B. Neubauer, V. Potin, A. Rosenauer, and M. Schowalter, Phys. Status Solidi C **0**, 1668 (2003).
[70] Y.-C. Cheng, E.-C. Lin, C.-M. Wu, C. C. Yang, J.-R. Yang, A. Rosenauer, K.-J. Ma, S.-C. Shi, L. C. Chen, C.-C. Pan, and J.-I. Chyi, Appl. Phys. Lett. **84**, 2506 (2004).

[71] D. Gerthsen, E. Hahn, B. Neubauer, A. Rosenauer, O. Schon, M. Heuken, and A. Rizzi, Phys. Status Solidi A **177**, 145 (2000).

[72] T. Li, E. Hahn, D. Gerthsen, A. Rosenauer, A. Strittmatter, L. Reibmann, and D. Bimberg, Appl. Phys. Lett. **86**, 241911 (2005).

[73] M. J. Galtrey, R. A. Oliver, M. J. Kappers, C. J. Humphreys, D. J. Stokes, P. H. Cliffton, and A. Cerezo, Appl. Phys. Lett. **90**, 061903 (2007).

[74] T. P. Bartel, P. Specht, J. C. Ho, and C. Kisielowski, Philos. Mag. **87**, 1983 (2007).

[75] M. Ferhat and F. Bechstedt, Phys. Rev. B **65**, 075213 (2002).

[76] J. Adhikari and D. A. Kofke, J. Appl. Phys. **95**, 4500 (2004).

[77] T. Takayama, M. Yuri, K. Itoh, T. Baba, and J. S. Harris, Jr., Jpn. J. Appl. Phys., Part 1 **39**, 5057 (2000).

[78] T. Takayama, M. Yuri, K. Itoh, and J. S. Harris, Jr., Appl. Phys. Lett. **90**, 2358 (2001).

[79] T. Saito and Y. Arakawa, Phys. Rev. B **60**, 1701 (1999).

[80] J. A. Purton, M. Y. Lavrentiev, and N. L. Allan, J. Mater. Chem. **15**, 785 (2005).

[81] S. Yu. Karpov, N. I. Podolskaya, I. A. Zhmakin, and A. I. Zhmakin, Phys. Rev. B **70**, 235203 (2004).